Eur. Phys. J. C (2025) 85:182
https://doi.org/10.1140/epjc/s10052-025-13903-w

THE EUROPEAN PHYSICAL JOURNAL C

Regular Article - Experimental Physics

Primary scintillation yields induced by α particles in gas mixtures of Argon/CF_4 at 9.5 bar

P. Amedo, S. Leardini, A. Saá-Hernández, D. González-Díaz[a]

Instituto Gallego de Física de Altas Energías, Universidad de Santiago de Compostela, Campus sur, Rúa Xosé María Suárez Núñez, s/n, 15782 Santiago de Compostela, Spain

Received: 24 October 2024 / Accepted: 4 February 2025

Abstract We report time and band -resolved scintillation from α-particles in Ar/CF_4 mixtures at a pressure of 9.5 bar. Our results show that %-level addition of CF_4 enables strong wavelength-shifted scintillation in the visible range, with yields at the level of 1000 ph/MeV, scintillation decay times of 9–25 ns and formation times well below 10 ns. Such a performance is a priori sufficient for accurate time-tagging of MeV-particles, without the need to resort to a pure noble gas, thus opening an appealing technological path for next-generation time projection chambers.

1 Introduction

Tetrafluoromethane (CF_4) is frequently used in particle physics instrumentation [1–6], one of the reasons being its strong VUV–visible scintillation strength of about 1000-3000 ph/MeV under ionizing radiation [7–10], around a factor of 10 shy of that in noble gases [11]. While this performance may seem modest, CF_4 enjoys a number of other remarkable features such as scintillation time constants below 15 ns [12] (considerably shorter than that of the triplet emission from noble gases [13,14]), high transparency down to VUV [15], and easiness of light collection and detection (most of its scintillation takes place in the range 200–800 nm [16]). It possesses a strong electron-cooling power [17] (hence, low diffusion) and, in admixtures with argon, it enables optical tracking down to minimum ionizing particles, through avalanche-induced scintillation [18]. Therefore, when considering detection systems that require the simultaneous detection of ionization and scintillation, and good track fidelity (see, e.g., [19] and references therein), CF_4 is arguably on a league of its own.

A subtler motivation to study systems based on CF_4 is the intriguing possibility that, in a way analogous to how 'Penning mixtures' enhance ionization [20,21], a suitable 'wavelength-shifting mixture' can potentially render scintillation strengths larger than those in the pure gas [22], shifting it to regions where it is easier to detect:

Penning transfer

$$A^{**} + B \rightarrow A + B^{+} + e^{-} \tag{1}$$

Gaseous wavelength-shifting

$$A^{**} + C \rightarrow A + C'^{,*} \rightarrow A + C' + h\nu \tag{2}$$

Here ** represents, generically, an excited state up to the ionization continuum and A, B, C, C' are atomic or molecular species. In the particular case of the UV emission of Ar-CF_4 mixtures, for example, A^{**} can be identified with one or several of the Ar 3^{rd} continuum precursors, $C'^{,*}$ is a highly excited molecular-ion state ($CF_4^{+,*}$) and C corresponds largely to the ground state of the molecular ion (CF_4^{+}). The visible component, on the other hand, can be assigned to transitions between CF_3^* states, while the A^{**} state has not been unambiguously identified. It could either be a high-lying Ar^{**} state, or the transfer reaction might require the formation of an intermediate species involving for instance an $ArCF_3^*$ exciplex [16,23,24].

Wavelength-shifting, when performed directly in gas phase instead of through solid converters (e.g., TPB [25], PEN [26]...) has other potential advantages: i) it can be expected to be more cost-effective and simpler to implement, and applicable even in trace-amount concentrations (e.g., [27]) and it) can provide a faster time response, given that it is not needed to wait for the A^{**} state to emit (e.g. [28]).

Compared to the body of knowledge amassed in regard to the CF_4 scintillation properties, the behaviour of CF_4 as

[a] e-mail: diego.gonzalez.diaz@usc.es (corresponding author)

Published online: 14 February 2025

a potential gaseous wavelength-shifter is much less studied, which is surprising since several experiments based on time projection chambers (TPCs) use or aim at making use of CF_4-based mixtures [29–32]. In fact, and to the best of the authors knowledge, no systematic studies of the primary scintillation yields seem to exist in literature, when CF_4 is used as a wavelength-shifter instead of as the main gas. A spectral analysis performed by our group in [16] allowed to address the strength of the transfer process 2 in the primary scintillation of Ar/CF_4 relative to pure Ar and CF_4 phases, for X-ray irradiation. That work shows for instance that 2%-addition of CF_4 to argon is sufficient to match the amount of visible scintillation in pure CF_4, with the yields increasing for higher concentrations up to 10%CF_4, at least. Based on the yields reported for pure CF_4, this observation would seemingly argue for scintillation strengths in the range of few 1000's ph/MeV for Ar/CF_4 mixtures too. The differences reported in [16] in the spectra of emission for α particles and X-rays (up to a factor $\times 3$ difference in the vis/uv ratios), however, and the absence of absolute-yield determinations for the latter study, preclude a direct estimate.

Our main motivation in this work is to assess the effectiveness of reactions of the type 2 in Ar/CF_4 admixtures, through a direct measurement of the scintillation yields and time profiles. We target specifically future neutrino experiments performed with pressurized argon TPCs (as presently intended by the DUNE collaboration [31,33], or under consideration for the upgrade of COHERENT [34]), for which we explored a range of CF_4 concentrations from 0.1% up to 10% (per volume), at a pressure around 10 bar. According to simulations performed in [35], an optical response in the range of 1000 ph/MeV with time constants of few 10's of ns would enable time tagging (T_0) with ns-level accuracy, in future neutrino detectors such as the high pressure TPC of DUNE's ND-GAr.

This paper comprises two main sections: Sect. 2 recalls our experimental setup and procedures in a succinct way, and Sect. 3 systematizes the main experimental results of our study. We end with our conclusions in Sect. 4.

2 Experimental setup and data analysis

Measurements were performed following a small adaptation of the device employed in [13]: a mini time projection chamber instrumented with a multi-wire readout, assembled in an all-CF/VCR gas system within a CF100 stainless-steel vessel, equipped with a recirculation system and purity-control. A schematic drawing can be seen in Fig. 1.

Compared to our earlier mini-TPC built and characterized thoroughly in Xe, the present one has been optimized for lower scintillation levels and therefore the drift-region was reduced to 0.7 cm. This brings the radioactive source closer to

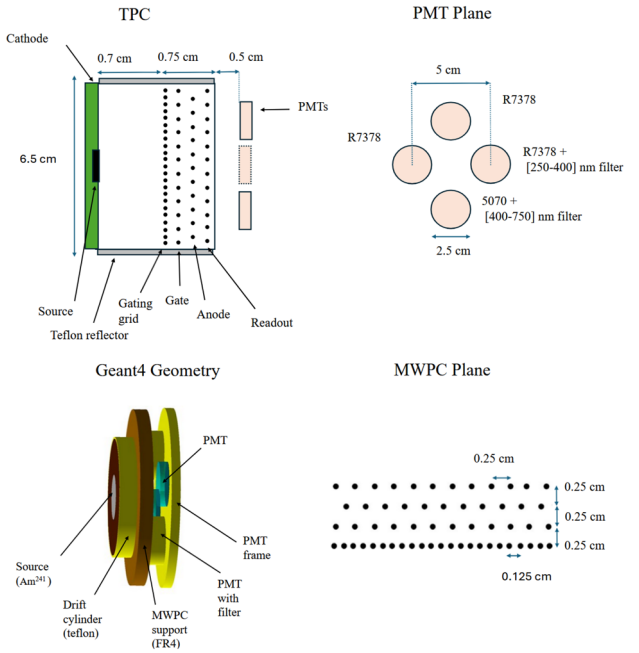

Fig. 1 Top-left: schematic drawing of the side-view of the setup used in this experiment, displaying the size of the relevant regions, the location of the PMTs and the source. Top-right: PMTs with their corresponding filters. Bottom left: Geant4 model of the setup. Bottom-right: scheme of the wire chamber. For a detailed description of the former iteration the reader is encouraged to check [13]

the optical system and eliminates the need for field-shapers. As in previous measurements, the chamber achieved a vacuum level of 10^{-3} mbar. The filling was done directly from the Ar and CF_4 bottles (purity 5 and 4.7, respectively) up to the desired pressure. Gas was recirculated to assure homogeneous mixing. It was verified during the campaign that the N_2 concentration levels were below 0.1% at all times, the sensitivity being limited by the background of the residual gas analyzer. It has been shown in [36] that CF_4 scintillation is robust up to N_2 concentrations as high as 4% (factor $\times 2$ drop), so we anticipate no purity issues in the conditions of this work.

The anode region was instrumented with thin wires to ensure good optical transparency towards the photosensor plane placed behind it. All four wire planes were made of a 99.95% purity tungsten core, plated with 99.99% purity gold. Anode wires had a diameter of 20 ± 2 μm and the rest of planes were assembled with 80 ± 8 μm -diameter ones. Anode and cathode wires have a pitch of 2.5 mm (shifted by half a pitch for each alternating plane), while the gating grid has a pitch of 1.25 mm. A metallic disk with an ^{241}Am deposit was housed in a circular groove at the middle of the TPC-cathode, leaving it flush with its surface and thus ensuring a minimal distortion of the electric field.

To increase sensitivity in the visible region compared to our earlier setup in [13], four pressure-resistant photomultipliers (PMs), model R7378 ($\times 3$) and 5070 ($\times 1$) from Hama-

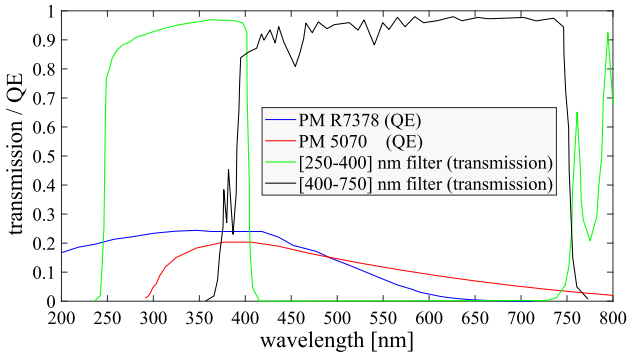

Fig. 2 Characteristics of the main optical elements used for the TPC readout. Three R7378 PMs from Hamamatsu (QE in blue) are used, one of them coupled to a UV-filter (green line). Measurements in the visible region are performed with a 5070 PM also from Hamamatsu, coupled to a visible-filter (black line)

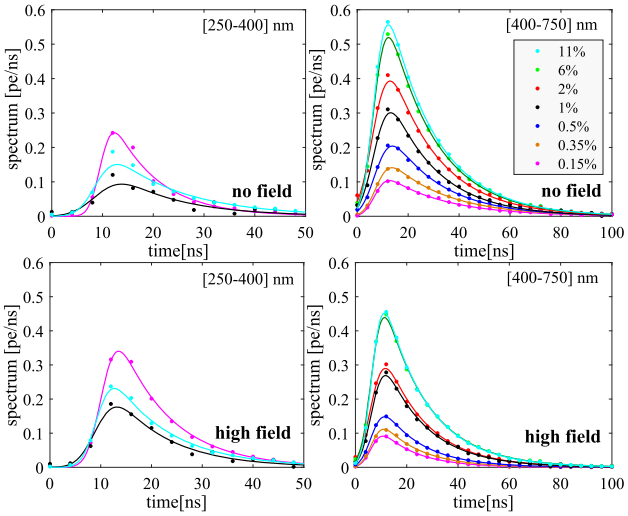

Fig. 3 Average waveforms obtained upon excitation with a ^{241}Am source, for different CF_4 concentrations (in photoelectrons per ns). Data is shown as circles. A fit to the convolution of a Gaussian time-response (from the PM) and an exponential decay (from the gas) is super-imposed. Left figures show the emission in the UV range and right figures the one in the visible range. Top row presents the results for no electric field and the bottom row for a pressure-reduced electric field around 100 V/cm/bar. The operating pressure is 9.5 bar, varying within 0.2 bar (maximum) from run to run. For the UV band the yield is weakly varying with CF_4 concentration (for an explanation see later in text), so only three representative concentrations are shown in order to avoid overcrowding

matsu, were assembled in a teflon frame and placed at close distance. A coincidence between two of the R7378 PMs was used to set the trigger, and data from the other two was used in the analysis. The trigger for the primary scintillation was set generally at the level of few photoelectrons. As the length of an α track is below 5 mm for argon at around 9.5 bar (much smaller than the dimensions of the optical system) events can be considered point-like for practical purposes and no trigger bias is anticipated. This was confirmed by triggering on the secondary scintillation signal and looking at the primary scintillation yields, that provided results compatible with the analysis presented here.

PM model R7378 was used, coupled to a band-pass UV-filter from Asahi ([250–400] nm), in order to assess the UV emission. The tandem covers most of the UV band of CF_4 and, with a nearly flat response at around 20–22%, it makes measurements in this range little dependent on the spectral content (Fig. 2, green and blue data). For the visible range, PM model 5070 coupled to a band-pass visible-filter ([400–750] nm), also from Asahi, was used (Fig. 2, black and red data). Quantum efficiencies were weighted with the spectra measured in [16] at 5 bar, yielding values of $QE_{uv} = 21\%$ and $QE_{vis} = 8.0\%$. Shape-variations of the spectra, in the range of CF_4 concentrations explored here, caused relative variations of less than 0.2% and 2% in the estimated QE's, respectively.

Data acquisition was performed with a CAEN DT5725 board of 14 bits, 125 MHz bandwidth and a sampling time of 4 ns. The acquisition window was set to 1 μs for S1 data and to 2 μs for S1-S2 combined data.[1] The latter runs were used to assess the overall consistency of the measurements, providing an independent study of the drift velocity and S1 yields. In them, the trigger was performed on the amplitude of the S2 signal, which is orders of magnitude bigger than the S1 signal. The setup was initially intended to offer a glimpse into the optical gains achievable in a MWPC system, however the obtained values of around 10 ph/e are probably limited due to the short distance between the MWPC plane and the Bragg peak of the alpha-track (down to few mm). Figure 3 presents (circles) an example of the average waveforms taken, in photoelectrons/ns, for conditions of no field and high field (around 100 V/cm/bar), at a pressure of 9.5 bar.

Data analysis was performed with Matlab scripts, including basic functions for pulse-shape analysis such as baseline corrections and waveform time-alignment to correct for offsets. Characteristic waveform parameters (signal rise-time, fall-time, amplitude, event barycenter, integrated charge) were then retrieved. The influence of applying cuts on those variables was studied, but their impact on the results found to be negligible. Calibration from PM charge (obtained from waveform integration) to photoelectrons was performed with a pulsed LED near the single-photon level (as described in [13]), and the influence of the PM response function on the time spectra modeled as:

$$\mathcal{F}(t) = (Ae^{-t/\tau_{UV(vis)}}) \circledast G(\sigma, t_o) \quad (3)$$

[1] We resort to a widely-used notation in the field of optical TPCs: S1 refers to the primary scintillation signal and S2 to the secondary scintillation one.

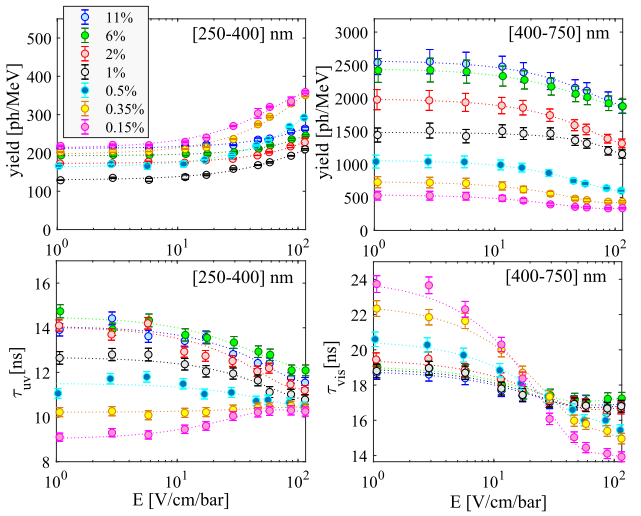

Fig. 4 Characteristics (absolute yield and decay time) of Ar/CF_4 scintillation as a function of the pressure-reduced electric field and CF_4 concentration. The top row shows the yields in the UV (left) and visible (right) bands. The bottom row shows the time constants. Following earlier works, the dependence with the electric field might be attributed to recombination, transferring energy from the $CF_4^{+,*}$ (UV) band to the CF_3^* (visible) one. Dashed lines are splines to guide the eye

Here $G(\sigma, t_o)$ is the PM time-response function under δ-excitation (assumed to be a Gaussian of width σ and offset t_0) and the symbol $\circledast$ denotes a convolution. With exception of UV data at low fields, average waveforms are well fitted to the above 'ansatz' (Fig. 3, lines). Despite a second time constant would make the fit better in this latter case, the difference was deemed too small and Eq. (3) was preserved for the sake of simplicity. In order to extract the yield parameter, the integrated signal was corrected by the PMT calibration and the collection efficiency, as described below.

3 Main results

Data was taken as a function of the electric field, and systematized from the fits to Eq. (3) in terms of scintillation yields and time constants, as shown in Fig. 4. The geometrical efficiency (probability of a photon landing on the PM photocathode) was estimated from Geant4 to be 0.0146 using the simulation framework developed in [13]. The overall uncertainty of the absolute normalization was estimated at 21% (15% from the single-photon calibration and 15% from the estimate of the geometrical efficiency). Moreover, a dedicated measurement was performed under pure xenon, by resorting to data from one of the unfiltered R7378 PMs (a single-PM trigger was sufficient in those conditions). The 2nd-continuum yields obtained in that reference run were compatible with the ones obtained in [13], within the given uncertainties.

Data in Fig. 4 displays a rich phenomenology, with the anti-correlation between UV and visible yields at high electric fields resembling early observations for pure CF_4 in [8], above 1 bar. In that work, such anticorrelation was naturally attributed to the scintillation stemming from charge recombination, moving energy from the $CF_4^{+,*}$ (UV) band into the CF_3^* (visible) one. Our data is compatible with that hypothesis: one can observe for instance that for the lowest-quenched mixtures, where electron diffusion is higher (e.g., for 0.15−0.35% CF_4 concentration), the yields in the visible region reach a plateau at the highest fields. For higher concentrations (lower diffusion) the maximum field applied in present conditions is not sufficient to reach the plateau of scintillation, suggesting that some recombination is still present and the effect is in fact stronger in that situation.

Time constants evolve greatly with electric field, too. For high field values, decay times in the visible band fit reasonably well to the range of τ = 10-15 ns reported in [12] for the CF_3^* scintillation in case of pure CF_4, at mildly-high pressure (3 bar). The elongation at low fields reported in that work is also reproduced here. The UV case is more complicated due to the existence of an interplay between the Ar 3rd continuum and $CF_4^{+,*}$ scintillation [16]. In fact, the observed time constants, despite being generally shorter than those in the visible, are much longer than the ones reported in [12] in the range [260–370] nm (τ = 5 ns). In both UV and visible bands, the increase of the time constants at low electric fields can be naturally interpreted due to additional recombination dynamics of the $CF_4^{+,*}$ ions and associated reactions. For the lowest concentrations, however, in case of the UV band (yellow and magenta circles in Fig. 4 bottom-left), it is likely that the contribution from the 3rd continuum plays a role too. A significant portion of that emission leaks into the [250–400] nm region [16], with a time constant around 5 ns [14]. Last, although the formation time of the scintillation precursors, be it through transfer reactions or recombination, is difficult to access in present conditions and specially given the prescription used in the fit, a safe upper bound of 10 ns (from 10% to 90% of the signal value) can be estimated from the waveforms of Fig. 3.

Figure 5 summarizes the main results of this work, providing the time constants and yields for the UV and visible bands at low and high electric fields.[2] The behaviour observed for the yields is similar to the one reported in [16] under X-rays, characterized by a sharp increase of the scintillation in the visible band up to an inversion point at around 10% CF_4. The presence of the 3rd continuum emission, on the other hand, leads to a compensatory effect on the UV yields: the minimum of scintillation is observed at around 1% CF_4 as the 3rd continuum is suppressed, followed by an increase with CF_4

[2] Experimental data and spline parameters are available under request to the authors.

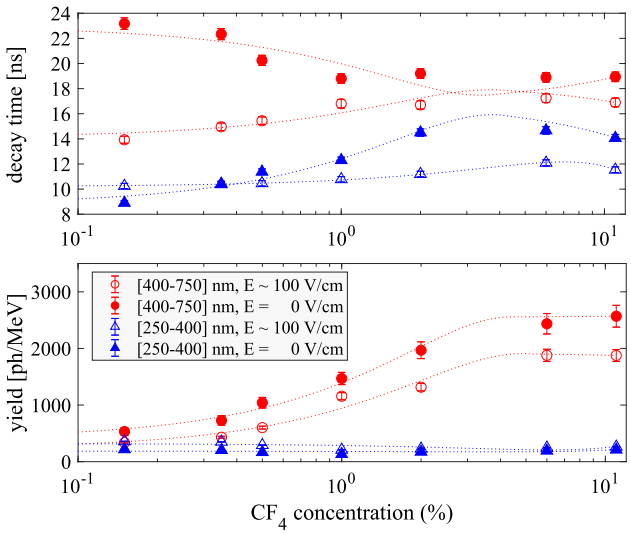

Fig. 5 Compilation of the main scintillation characteristics of Ar/CF_4 mixtures under α particles from ^{241}Am and at 9.5 bar, as a function of CF_4 concentration. Red symbols are used for measurements in the visible band and blue for the UV one. Solid symbols correspond to low-field measurements and open ones indicate high field. Top: decay times. Bottom: scintillation yields in ph/MeV. Dashed lines are splines to guide the eye

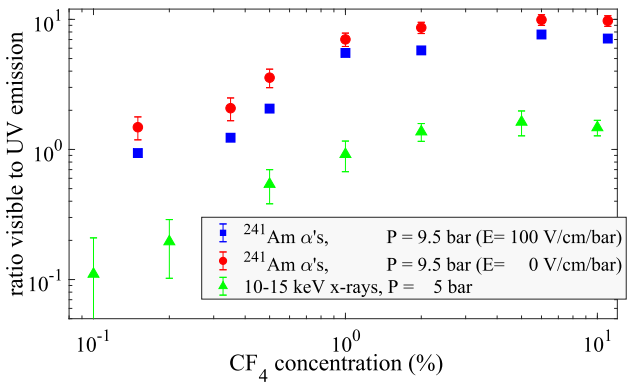

Fig. 6 Ratio between scintillation in the visible and uv bands (vis/uv), defined in the range [400–750] nm and [250–400] nm. Blue (high field) and red (low field) markers show the results in this work for α particles (9.5 bar), while green markers show the result from previous measurements under X-rays (5 bar). The 'ratio of ratios', $\mathcal{R}_{\alpha/x}$, stays at $4.6 \pm 0.8(\text{sta}) \pm 1.4(\text{sys})$, compatible with earlier results

concentration as the population of $CF_4^{+,*}$ increases. In the range explored, the UV yields change by less than a factor of 2. With the caveat discussed below, on the observed particle-dependence of CF_4 scintillation, the reader is encouraged to consult [16] for a microscopic interpretation of the observed trends.

Despite reproducing the concentration trends measured in X-ray data, the ratio of the yields in the visible and UV bands (vis/UV) that is observed under α particles in these measurements tops at nearly 10, much higher than the one observed for X-rays in [16]. A comparison is shown in Fig. 6, displaying the ratio:

$$\mathcal{R}_{\alpha/x} = \frac{\text{vis/uv}|_{\alpha, E=100}}{\text{vis/uv}|_x} = 4.6 \pm 0.8 \tag{4}$$

(in case of α particles the ratio is taken at high fields, to minimize the impact of recombination). Upon including the systematic uncertainty on present measurements, the estimate is $\mathcal{R}_{\alpha/x} = 4.6 \pm 0.8(sta) \pm 1.4(sys)$ for Ar-CF_4 mixtures. Despite the different operating pressure, this result would hint at compatibility with earlier values of $\mathcal{R}_{\alpha/x} = 2.8 \pm 0.3$ for spectral measurements performed for pure CF_4 in the pressure range 1–3 bar, once recombination is excluded (see [16] and [8], [12]). In all, present measurements further support the evidence of α particles leading to substantially higher vis/uv scintillation ratios compared to X-rays, and make it compelling to address the scintillation spectra of these mixtures under minimum ionizing radiation in the future.

4 Conclusions

We have presented time and band-resolved measurements of the primary scintillation of Ar/CF_4 mixtures under α-particle irradiation, at a pressure of 9.5 bar. The results are of potential interest to next-generation TPCs for neutrino physics, in which time stamping through primary scintillation is a valuable asset, needed to properly assign the time of the interaction to the neutrino beam. Our results show that, upon the mere addition of 1%CF_4 to argon, scintillation yields in the range 1400–1200 ph/MeV can be obtained, in the range of pressure-reduced electric fields of 40–100 V/cm/bar. The emission takes place predominantly in the [400–750] nm band, easily accessible to silicon-based photosensors. The decay constant of the scintillation is much shorter than that of noble gases, in the range of τ = 14-17 ns, thus showing good prospects for timing. Our measurements confirm earlier results obtained under X-rays, in regard to the gaseous wavelength-shifting capabilities of CF_4 when added to argon. The discrepancy between the intensity in the visible and UV bands as observed for α's and X-rays, $\mathcal{R}_{\alpha/x} = 4.6 \pm 0.8(sta) \pm 1.4(sys)$, is compatible with previous observations for pure CF_4. It makes a compelling case for the measurement of scintillation under minimum ionizing particles and α's in the same conditions.

Acknowledgements Special thanks to Alan Bross, Carlos Escobar and Adam Para (Fermilab) for continuous encouragement and many insightful discussions.

Funding This research has received financial support from the European Union's Horizon 2020 Research and Innovation programme under GA no. 101004761, from Xunta de Galicia (Centro singular de inves-

tigación de Galicia, accreditation 2019-2022), and by the "María de Maeztu" Units of Excellence program MDM-2016-0692. DGD was supported by the Ramón y Cajal program (Spain) under contract number RYC-2015-18820. This research was also partly funded by the Spanish Ministry ('Proyectos de Generación de Conocimiento', PID2021-125028OB-C21).

Data Availability Statement Data will be made available on reasonable request. [Author's comment: The datasets generated during and/or analysed during the current study are available from the corresponding author on reasonable request.]

Code Availability Statement Code/software will be made available on reasonable request. [Author's comment: The code/software generated during and/or analysed during the current study is available from the corresponding author on reasonable request.]

Funded by SCOAP[3].

References

1. J.B. Battat, C. Deaconu, G. Druitt, R. Eggleston, P. Fisher, P. Giampa, V. Gregoric, S. Henderson, I. Jaegle, J. Lawhorn, J.P. Lopez, J. Monroe, K.A. Recine, A. Strandberg, H. Tomita, S. Vahsen, H. Wellenstein, Nucl. Instrum. Methods Phys. Res. Sect. A Accel. Spectrom. Detect. Assoc. Equip. **755**, 6 (2014). https://doi.org/10.1016/j.nima.2014.04.010
2. A. Roberts, P. Svihra, A. Al-Refaie, H. Graafsma, J. Küpper, K. Majumdar, K. Mavrokoridis, A. Nomerotski, D. Pennicard, B. Philippou, S. Trippel, C. Touramanis, J. Vann, J. Instrum. **14** (2019). https://doi.org/10.1088/1748-0221/14/06/P06001
3. F.A.F. Fraga, L.M.S. Margato, S.T. Fetal, M.M.F.R. Fraga, R. Ferreira-Marques, A.J.P.L. Policarpo, B. Guerard, A. Oed, G. Manzini, T. van Vuure, Nucl. Instrum. Methods A **478**, 357 (2002). https://doi.org/10.1016/S0168-9002(01)01829-0
4. M. Takahashi, S. Kabuki, K. Hattori, N. Higashi, S. Iwaki, H. Kubo, S. Kurosawa, K. Miuchi, K. Nakamura, H. Nishimura, J.D. Parker, T. Sawano, A. Takada, T. Tanimori, K. Taniue, K. Ueno, Nucl. Instrum. Methods Phys. Res. Sect. A Accel. Spectrom. Detect. Assoc. Equip. **628**, 150 (2011). https://doi.org/10.1016/j.nima.2010.06.305
5. R. Forty, Nucl. Instrum. Methods Phys. Res. Sect. A Accel. Spectrom. Detect. Assoc. Equip. **433**, 257 (1999). https://doi.org/10.1016/S0168-9002(99)00310-1
6. M. Fraga, F. Fraga, S. Fetal, L. Margato, R. Marques, A. Policarpo, Nucl. Instrum. Methods Phys. Res. Sect. A Accel. Spectrom. Detect. Assoc. Equip. **504**, 88 (2003). https://doi.org/10.1016/S0168-9002(03)00758-7
7. A. Pansky, A. Breskin, A. Buzulutskov, R. Chechik, V. Elkind, J. Va'vra, Nucl. Inst. Methods Phys. Res. A **354**, 262 (1995). https://doi.org/10.1016/0168-9002(94)01064-1
8. A. Morozov, M.M. Fraga, L. Pereira, L.M. Margato, S.T. Fetal, B. Guerard, G. Manzin, F.A. Fraga, Nucl. Instrum. Methods Phys. Res. Sect. A Accel. Spectrom. Detect. Assoc. Equip. **268**, 1456 (2010). https://doi.org/10.1016/j.nimb.2010.01.012
9. B. Azmoun, A. Caccavano, M. Rumore, J. Sinsheimer, N. Smirnov, S. Stoll, C. Woody, IEEE Trans. Nucl. Sci. **57**, 2376 (2010). https://doi.org/10.1109/TNS.2010.2052632
10. G. Lehaut, S. Salvador, J.M. Fontbonne, F.R. Lecolley, J. Perronnel, C. Vandamme, Nucl. Instrum. Methods Phys. Res. Sect. A Accel. Spectrom. Detect. Assoc. Equip. **797**, 57 (2015). https://doi.org/10.1016/j.nima.2015.05.050
11. K. Saito, H. Tawara, T. Sanami, E. Shibamura, S. Sasaki, IEEE Trans. Nucl. Sci. **49 I**, 1674 (2002). https://doi.org/10.1109/TNS.2002.801700
12. A. Morozov, M. Fraga, L. Pereira, L. Margato, S. Fetal, B. Guerard, G. Manzin, F. Fraga, Nucl. Instrum. Methods Phys. Res. Sect. A Accel. Spectrom. Detect. Assoc. Equip. **628**, 360 (2011). https://doi.org/10.1016/j.nima.2010.07.001
13. S. Leardini, E.S. García, P. Amedo, A. Saa-Hernández, D. González-Díaz, R. Santorelli, D.J. Fernández-Posada, D. González, Eur. Phys. J. C **82**, 425 (2022). https://doi.org/10.1140/epjc/s10052-022-10385-y
14. R. Santorelli, E.S. Garcia, P.G. Abia, D. González-Díaz, R.L. Manzano, J.J. Morales, V. Pesudo, L. Romero, Eur. Phys. J. C **81**, 622 (2021). https://doi.org/10.1140/epjc/s10052-021-09375-3
15. H. Keller-Rudek, G.K. Moortgat, R. Sander, R. Sörensen, Earth Syst. Sci. Data **5**, 365 (2013). https://doi.org/10.5194/essd-5-365-2013
16. P. Amedo, D. González-Díaz, F.M. Brunbauer, D.J. Fernández-Posada, E. Oliveri, L. Ropelewski, Front. Detect. Sci. Technol. **1** (2023). https://doi.org/10.3389/fdest.2023.1282854
17. L.G. Christophorou, J.K. Olthoff, *Fundamental Electron Interactions with Plasma Processing Gases* (Springer US, 2004). https://doi.org/10.1007/978-1-4419-8971-0
18. P. Amedo, R. Hafeji, A. Roberts, A. Lowe, S. Ravinthiran, S. Leardini, K. Majumdar, K. Mavrokoridis, D. González-Díaz, J. Instrum. **19**, C05001 (2024). https://doi.org/10.1088/1748-0221/19/05/C05001
19. D. González-Díaz, F. Monrabal, S. Murphy, Nucl. Instrum. Methods Phys. Res. Sect. A Accel. Spectrom. Detect. Assoc. Equip. **878**, 200 (2018). https://doi.org/10.1016/j.nima.2017.09.024
20. Ö. Şahin, I. Tapan, N. Özmutlu, R. Veenhof, J. Instrum. **5**, P05002 (2010). https://doi.org/10.1088/1748-0221/5/05/P05002
21. Ö. Şahin, T.Z. Kowalski, T. Murakami, K. Niemi, T. Gans, R. Veenhof, J. Instrum. **11**, P01003 (2016). https://doi.org/10.1088/1748-0221/11/01/P01003
22. T. Főrster, Discuss. Faraday Soc. **27**, 7 (1959). https://doi.org/10.1039/DF9592700007
23. L.C. Lee, X. Wang, M. Suto, J. Chem. Phys. **85**, 6294 (1986). https://doi.org/10.1063/1.451459
24. M. Suto, N. Washida, H. Akimoto, M. Nakamura, J. Chem. Phys. **78**, 1019 (1983). https://doi.org/10.1063/1.444901
25. C. Benson, G.O. Gann, V. Gehman, Eur. Phys. J. C **78** (2018). https://doi.org/10.1140/epjc/s10052-018-5807-z
26. M. Kuźniak, D. González-Díaz, P. Amedo, C.D. Azevedo, D.J. Fernández-Posada, M. Kuźwa, S. Leardini, A. Leonhardt, T. Łcki, L. Manzanillas, D. Muenstermann, G. Nieradka, R. de Oliveira, T.R. Pollmann, A. Saá-Hernández, T. Sworobowicz, C. Türkoğlu, S. Williams, Eur. Phys. J. C **81**, 1 (2021). https://doi.org/10.1140/EPJC/S10052-021-09316-0
27. DUNE collaboration, J. Instrum. **19**, P08005 (2024). https://doi.org/10.1088/1748-0221/19/08/P08005
28. E. Segreto, Phys. Rev. C **91**, 035503 (2015). https://doi.org/10.1103/PhysRevC.91.035503
29. S.E. Vahsen, C.A.J. O'Hare, W.A. Lynch, N.J.C. Spooner, E. Baracchini, P. Barbeau, J.B.R. Battat, B. Crow, C. Deaconu, C. Eldridge,

A.C. Ezeribe, M. Ghrear, D. Loomba, K.J. Mack, K. Miuchi, F.M. Mouton, N.S. Phan, K. Scholberg, T.N. Thorpe. Cygnus: feasibility of a nuclear recoil observatory with directional sensitivity to dark matter and neutrinos (2020). https://doi.org/10.48550/arXiv.2008.12587

30. H.M. Araújo, S.N. Balashov, J.E.B.F.M. Brunbauer, C. Cazzaniga, C.D. Frost, F. Garcia, A.C. Kaboth, M. Kastriotou, I. Katsioulas, A. Khazov, H. Kraus, V.A. Kudryavtsev, S. Lilley, A. Lindote, D. Loomba, M.I.L.E.L. Asamar, P.L.D.P.A. Majewski, T. Marley, C. McCabe, A.F. Mills, M. Nakhostin, T. Neep, F. Neves, K. Nikolopoulos, E. Oliveri, L. Ropelewski, E. Tilly, V.N. Solovov, T.J. Sumner, J.T.R. Turnley, M.G.D. van der Grinten, R. Veenhof, Astropart. Phys. **151**, 102853 (2022). https://doi.org/10.1016/j.astropartphys.2023.102853
31. DUNE collaboration, A gaseous argon-based near detector to enhance the physics capabilities of dune (2022). https://doi.org/10.48550/arXiv.2203.06281
32. M. Cortesi, H. Sims, J. Pereira, Y. Ayyad, P. Majewski, I. Katsioulas, J. Instrum. **18**, P08005 (2023). https://doi.org/10.1088/1748-0221/18/08/P08005
33. DUNE collaboration, Dune phase ii: Scientific opportunities, detector concepts, technological solutions (2024). https://doi.org/10.48550/arXiv.2408.12725
34. J. Asaadi, P.S. Barbeau, B. Bodur, A. Bross, E. Conley, Y. Efremenko, M. Febbraro, A. Galindo-Uribarri, S. Gardiner, D. Gonzalez-Diaz, M.P. Green, M.R. Heath, S. Hedges, J. Liu, A. Major, D.M. Markoff, J. Newby, D.S. Parno, D. Pershey, R. Rapp, D.J. Salvat, K. Scholberg, L. Strigari, B. Suh, R. Tayloe, Y.T. Tsai, S.E. Vahsen, T. Wongjirad, J. Zettlemoyer. Physics opportunities in the ornl spallation neutron source second target station era (2022).
35. A. Saá-Hernández, D. González-Díaz, J. Martín-Albo, M. Tuzi, P. Amedo, J. Baldonedo, C. Benítez, S. Bounasser, E. Casarejos, J. Collazo, A. Fernández-Prieto, D.J. Fernández-Posada, S. Leardini, D. Rodas-Rodríguez, A.L. Saborido, A. Segade, A. Slatera. On the determination of the interaction time of gev neutrinos in large argon gas tpcs (2024). arXiv:2401.09920
36. L.M. Margato, A. Morozov, L. Pereira, M.M. Fraga, F.A. Fraga, Nucl. Instrum. Methods Phys. Res. Sect. A Accel. Spectrom. Detect. Assoc. Equip. **695**, 425 (2012). https://doi.org/10.1016/j.nima.2011.10.033